Toxicology 465 (2022) 153044

Contents lists available at ScienceDirect

Toxicology

journal homepage: www.elsevier.com/locate/toxicol

Per- and polyfluoroalkyl substances (PFAS) augment adipogenesis and shift the proteome in murine 3T3-L1 adipocytes

Seyed Mohamad Sadegh Modaresi, Wei Wei, Marques Emily, Nicholas A. DaSilva, Angela L. Slitt *

Department of Biomedical and Pharmaceutical Sciences, University of Rhode Island, Kingston, RI, 02881, USA

ARTICLE INFO

Handling Editor: Thomas Knudsen

Keywords:
Adipogenicity
Proteomics
PFAS

ABSTRACT

The Per- and polyfluoroalkyl substances (PFAS) are a wide group of fluorinated compounds, which the health effects of many of them have not been investigated. Perfluorinated sulfonates, such as perfluorooctane sulfonate (PFOS) and perfluorinated carboxylates, such as perfluorooctanoic acid (PFOA) are members of this broad group of PFAS, and previous studies have shown a correlation between the body accumulation of PFOS and PFOA and increased adipogenesis. PFOA and PFOS have been withdrawn from the market and use is limited because of their persistence, toxicity, and bioaccumulative properties. Instead, short chain PFAS have been created to replace PFOA and PFOS, but the health effects of other short chain PFAS are largely unknown. Therefore, herein we aimed to comprehensively determined the potential adipogenesis of ten different PFAS (PFBS, PFHxS, PFOS, PFBA, PFHxA, PFHA, PFOA, PFNA, PFDA, and HFPO-DA) and investigated the differences in protein expression of 3T3-L1 cells upon exposure to each PFAS. 3T3-L1 cells were differentiated with or without each PFAS for 4-days, and cellular lipid was quantified using Nile Red staining. Analysis of the adipocyte proteome was performed to identify the pathways related to adipogenesis and quantify proteins significantly affected by each PFAS. The results showed that in general, every PFAS investigated in our study has the potential to induce the 3T3-L1 differentiation to adipocytes in the presence of rosiglitazone, with the concentrations that range between 0.25 and 25 μM. Proteomics analysis revealed specific markers regarding to adipogenesis upregulated upon exposure to each of the ten PFAS.

1. Introduction

Per- and polyfluoroalkyl substances (PFAS) are a diverse group of synthetic chemicals that are used vastly in commercial applications ranging from fire-fighting foams, insecticide formulations, coatings for fabrics, leather, and carpet to grease-proof paper products for food packaging (Renner, 2001; Glüge et al., 2020). These compounds are thermally and chemically stable and are not readily degraded at high temperature or by acids, alkalis, and oxidizing agents (Olsen et al., 2017). These properties are responsible for their usefulness in industrial and consumer products, yet also render PFAS as a source of persistent contamination in the environment (Yamashita et al., 2005). Two major groups of PFAS include the perfluorinated carboxylic acid and sulfonic acid series that are fully fluorinated. Perfluorooctane sulfonate (PFOS) and perfluorooctanoate (PFOA) are among the most studied PFAS because of their extensive use, persistence, and long serum half lives in humans (Olsen et al., 2007). The elimination half-lives of PFAS are significantly different across compounds and are dependent on species and sex. According to latest US Agency for Toxic Substances and Disease Registry update, the estimated elimination half-lives in humans are 2.1–10.1 years for PFOA and 3.3–27 years for PFOS (ATSDR, 2021). PFOS and PFOA have been phased out of use and production in the US in 2002 and 2005, respectively. However, many alternative short chain PFAS are still widely used and are unregulated; less is known about the risk of alternative short chain PFAS to human health. Perfluorobutane sulfonic acid (C4, PFBS) and perfluorohexane sulfonic acid (C6, PFHxS) are among the short chain alternatives of PFOS; and perfluorobutanoic acid (C4, PFBA) and perfluorohexanoic acid (C6, PFHxA) are among the short chain alternatives of PFOA. Generally, the blood half-lives of PFAS increase with chain length for carboxylates, and they are shorter for branched isomers (Danish Ministry of the Environment, 2015). Despite the relative lack of data available on the short-chain PFAS it has often

* Corresponding author at: University of Rhode Island, 395D, Avedisian Hall, 7 Greenhouse Rd., Kingston, RI, 02881, USA.
E-mail address: aslitt@uri.edu (A.L. Slitt).

https://doi.org/10.1016/j.tox.2021.153044
Received 27 July 2021; Received in revised form 27 October 2021; Accepted 16 November 2021
Available online 17 November 2021

been assumed that they will cause similar or lesser effects than PFOS because of their short half-lives. This was demonstrated in a study where the doses of PFBS needed to generate same increases in the enzyme hepatic acyl CoA oxidase activity, which is a measure of liver proliferation was almost 50 times higher than those of PFOS and PFHxS (Lau et al., 2007). Moreover, the relation between different PFAS levels in human plasma with metabolic syndrome has been investigated, and PFNA is consistently associated with increased risk for components of metabolic syndrome (Christensen et al., 2019).

Obesity has become a pandemic problem that impacts all people of different ethnicities, ages and in all parts of the world, both in developed western countries and in poorer nations. It is associated with other diseases such as type 2 diabetes mellitus, fatty liver disease, hypertension and cardiovascular diseases (Antipatis and Gill, 2001; Blüher, 2019). The potential endocrine disrupting effects of different long and short chain PFAS on humans are largely unknown. There is evidence suggesting that rise in obesity is correlated with the significant increase in the number of industrial chemicals including PFAS available on the market (Baillie-Hamilton, 2002; Liu et al., 2018). Little is known regarding emerging PFAS as potential obesogens or chemicals that induce expansion of adipose tissue through adipogenesis. Adipogenesis is a series of cellular signals that cause undifferentiated fibroblasts to differentiate into adipocytes. Multiple signaling pathways are involved in adipogenic pathogenesis such as insulin signaling pathway, Peroxisome proliferator-activated receptor (PPAR) regulation, adenosine monophosphate-activated kinase (AMPK) pathway, and glucose pathway (Guru et al., 2021). It is a cellular process that has three distinct stages: (i) commitment of mesenchymal stem cells to the adipocyte lineage; (ii) replication of DNA and cells proliferation, which is called mitotic clonal expansion (MEC); (iii) terminal differentiation in which there is an increase in expression of genes and transcriptional factors such as CCAAT/enhancer-binding proteins (C/EBPs) family and PPARγ – and a substantial enhancement in lipogenesis and induction of lipogenic genes such as acetyl CoA carboxylase (ACC), fatty acid synthase (FAS), adipocyte fatty acid binding protein (aP2), leptin (Lep), and adiponectin (Ahmad et al., 2020). PPARs belong to the nuclear receptor family and play a crucial role in regulating metabolic homeostasis and inflammation. PPARγ agonists, such as thiazolidinediones (TZDs), are prescribed mainly as antidiabetic drugs. TZDs cause an increase in the potency of the whole-body insulin sensitivity, in part through adipose tissue expansion. The molecular basis of adipocyte-specific gene expression is not well understood. The studies have shown PPARγ levels are significantly increased during the differentiation of preadipocytes to adipocytes (Chawla et al., 1994). First, adipocyte regulatory factor 6 (ARF6) was identified as differentiation dependent nuclear factor that binds to adipocyte protein 2 (aP2) gene enhancer. Then PPARγ2 was cloned as a component of ARF6, which confers adipocyte-specific expression to the murine adipocyte protein 2 (aP2) gene through different adipose regulatory elements (Tontonoz et al., 1994). The study identified adipose regulatory elements as hormone response elements for PPAR and that the PPARγ/RXRα heterodimer functions as a transactivator of the adipose regulatory factor-6 complex. Subsequently, PPAR response elements were found in many adipocyte genes (Rangwala and Lazar, 2000). Also, small lipophilic ligands are structurally related to PPARγ and there has been interest in identifying ligands for the receptor. The ligands can be synthetic or naturally occurring and in the presence of both PPARγ and RXRα ligands, a synergistic effect is observed (Schulman et al., 1998). As previously mentioned, he most potent ligands for PPARγ are the thiazolidinediones (TZDs) which have been approved as a class of antidiabetic pharmaceutics (Ciaraldi et al., 2002). Several lipid species have been introduced as endogenous ligands which activate PPARγ (Itoh et al., 2008). Moreover, it has been found that PPARγ might also be a target of PFAS. The study reported that multiple PFAS were able to activate human PPARγ and provided the evidence for the direct interaction of PFAS with hPPARγ-LBD in ligand-receptor binding assay (Zhang et al., 2014). Overall, the number of pathways, cofactors, metabolites, and modifications that are involved in regulating PPARγ shows the level of complexity of the adipogenic program of gene transcription.

Table 1
PFAS information used for hepatocytes treatments.

PFAS	Chemical name	CAS #	Purity (%)	Catalog# (Lot)
PFBS (C4s)	Perfluorobutane sulfonic acid	375-73-5	100	S-74451 (27461)
PFHxS (C6s)	Potassium perfluorohexanesulfonate	3871-99-6	98	S-17292 M (21279)
PFOS (C8s)	Potassium perfluorooctanesulfonate	2795-39-3	98	PFOS-002 N (24187)
PFBA (C4)	Perfluorobutanoic acid	375-224	98	S-17292 K (21247)
PFHxA (C6)	Perfluorohexanoic acid	307-24-2	97.0	S-17292B (21241)
PFHA (C7)	Perfluoroheptanoic acid	375-85-9	99.0	S-17292C (21242)
PFOA (C8)	Perfluorooctanoic acid	335-67-1	100.0	PFOA-001 N (27462)
PFNA (C9)	Perfluorononanoic acid	375-95-1	97.0	S-17292E (21243)
PFDA (C10)	Perfluorodecanoic acid	335-76-2	98.0	S-17292 F (21244)
HFPO-DA (GenX)	Perfluoro(2-methyl-3-oxahexanoic) acid	13252-13-6	95.7	S-17292 T (28563)

Ten different PFAS were selected for the study based on their chemical structure, and their exposure to human, wildlife, and environment.

The purpose of this work was to evaluate the adipogenicity potential of PFBS, PFHxS, PFOS, PFBA, PFHxA, PFHA, PFOA, PFNA, PFDA, and HFPO-DA on differentiated or undifferentiated 3T3-L1 cells in the presence or absence of rosiglitazone. Hexafluoropropylene oxide dimer acid (HFPO-DA) with the trade name of GenX is an industrial replacement for the long straight chain PFOA following its phase out (Conley et al., 2021). Moreover, rosiglitazone, differentiating compounds in culture media, and PFAS were used with three different concentrations to investigate the adipogenesis potential of all the factors involved. The preadipose cell line 3T3-L1 which have a well known potential to differentiate from fibroblasts to adipocytes have been originally developed from murine Swiss 3T3 cells and they are widely used for studying adipogenicity potential of different compounds and identifying the targets involved (Green and Kehinde, 1974). These PFAS were selected based on detection in humans (Kotlarz et al., 2020), birds and pilot whales (Dassuncao et al., 2019), and in private well water (Domingo and Nadal, 2019). Additionally, protein expression profiling performed to elucidate the mechanisms and signaling pathways involved in adipogenesis upon PFAS exposure. Given that PFAS are the activators of PPARγ, we hypothesized that PFAS will induce cellular lipid content within differentiated and undifferentiated 3T3-L1 preadipocytes.

2. Materials and methods

2.1. Test chemicals

All ten PFAS evaluated (PFBS, PFHxS, PFOS, PFBA, PFHxA, PFHA, PFOA, PFNA, PFDA, and HFPO-DA) are described in Table 1 and were purchased from AccuStandard Inc. (New Haven, CT, USA) and dissolved in dimethyl sulfoxide (DMSO; Sigma Aldrich, St. Louis, MO), rosiglitazone (ROSI; Cayman, Ann Arbor, Michigan) and 3-Isobutyl-1-methylxanthine (IBMX; Sigma Aldrich, St. Louis, MO) were prepared in DMSO. Dexamethasone and insulin solutions were purchased from Sigma Aldrich (St. Louis, MO). All chemicals and solvents were obtained from Sigma Aldrich (St. Louis, MO) or Thermo Fisher Scientific (Waltham, MA) unless specified otherwise.

Table 2
The components and concentration of differentiating cocktail.

	1 X	0.5 X	0.25 X
Rosiglitazone	50 nM	25 nM	12.5 nM
IBMX	50 nM	25 nM	12.5 nM
DEXM	25 nM	12.5 nM	6.25 nM
Insulin	1 ug/mL	0.5 ug/mL	0.25 ug/mL

The 3T3-L1 cells were treated with differentiating cocktail at three different concentrations during differentiation to adipocytes.

2.2. 3T3-L1 pre-adipocyte cell culture, differentiation, and treatment

Mouse 3T3-L1 fibroblasts (Zen-Bio, SP-L1-F) were obtained from Zen-Bio (Durham, NC) and were cultured and differentiated according to Zen-Bio Cell Care Manual. Cells were cultured in 96 well plates for the adipogenesis study and 12 well plates (Corning Life Sciences, ME) for proteomic evaluation, and the number of cells per well was 5000 per cm^2. 3T3-L1 pre-adipocytes were cultured with Dulbecco's Modified Eagle's Medium, high glucose (DMEM) and supplemented with 10 % newborn calf serum (NCS) and 100U/mL penicillin and 100 ug/mL streptomycin (1 % P/S). 48 h post-confluency, cell differentiation was induced with an appropriate volume for the cell culture vessel of differentiation medium-I (DMI) with initial treatment for 2 days. Differentiation medium-I was comprised of DMEM containing 10 % fetal bovine serum (FBS), 1 % P/S, IBMX, Dexamethasone, insulin, with or without rosiglitazone. The differentiating cocktail was then diluted and the concentration of differentiating compounds were referred to as 1 X, 0.5 X and 0.25 X. The concentration of the chemicals including rosiglitazone for each dilution has been summarized in Table 2. The rationale for culturing with different concentrations of the differentiating cocktail was so that the activity of the cocktail did not maximally induce adipogenesis and overwhelm the induction potential of the PFAS evaluated. Concentrations for the individual PFAS (PFBS, PFHxS, PFOS, PFBA, PFHxA, PFHA, PFOA, PFNA, PFDA, and HFPO-DA) treatments was 0.25 μM, 2.5 μM, 25 μM or Vehicle (0.1 % DMSO).

After two days of initial differentiation and treatment, cell media was replaced with differentiation medium-II (DMII), comprised of DMEM containing 10 % fetal bovine serum (FBS), 1 % P/S, and 1 μg/mL insulin, plus corresponding concentration of PFAS treatment. After 2 days in DMII with PFAS treatments, cells were fixed with 10 % formalin and then stained with Nile Red and DAPI. The study outline has been summarized in Fig. 1.

For protein analysis, the PFAS concentration of 25 μM and differentiating cocktail dilution of 1X with ROSI was selected based on Nile-red staining results. Protein was isolated in RIPA buffer and protein concentrations were determined by the BCA protein assay kit (ThermoFisher Scientific, Waltham, MA).

2.3. Nile red staining and lipid quantification

Nile Red (Sigma Aldrich, St. Louis, MO) was reconstituted in DMSO (3.1 mM) and aliquoted to avoid freeze thaw cycles. A fresh working solution was prepared at a final concentration of 3.1 μM in phosphate buffered saline (PBS). Cells were washed with 1X PBS and fixed with 10 % formalin for 10−15 min at room temperature. After fixing, cells were washed with 1X PBS and the Nile Red working solution was added for 10−15 min. Subsequently, cells were washed with 1X PBS for 2 times and a DAPI (4′,6-diamidino-2-phenylindole) working solution (300 nM in PBS) was added as a counterstain for 5 min. After finishing the staining, cells were then washed with PBS 2 times and ready for lipid quantification with a SpectroMax M2 plate reader (Molecular Devices, San Jose, CA) with excitation and emission wavelengths of 485/535 nm for Nile Red and 358/461 nm for DAPI.

2.4. Sample preparation for SWATH-MS

Samples were prepared, using a similar method as Marques et al. (2020). In brief, the cells were homogenized in 500 μL of RIPA buffer following the manufacturer's instructions. Samples were then spun at 7000×g for 10 min and the supernatant was collected. The Pierce BCA protein assay kit (ThermoFisher Scientific, Waltham, MA) was used according to manufacturer's protocols to determine the total protein concentration of the samples. For proteomics, 3 12-well plates were used, and each treatment group was compared to their own control to take into account inter-plate variability. After spiking samples (~80 μg protein) with 2 μg bovine serum albumin (BSA), the protein samples were digested. First, 25 μL DTT (100 mM) was added and incubated at 35 °C for 30 min in a shaking water bath (120 rpm). Then, sample alkylation was performed in the dark with 25 μL IAA (200 mM) for 30 min at RT. Proteins were precipitated and concentrated using cold water, methanol and chloroform (1:2:1), and centrifugation at 10,000 rpm, 5 min at 10 °C. After washing protein pellet with ice-cold methanol, it was suspended in 100 μL of 50 mM ammonium bicarbonate (pH ~8) containing 3 % w/v sodium deoxycholate (DOC). Next, trypsin treated with N-tosyl-L-phenylalanine chloromethyl ketone (TPCK) (4 μg) was added to samples at a ratio of 1:20 (trypsin: protein) and samples were transferred into digestion tubes (PCT MicroTubes, Pressure Biosciences Inc., Easton, MA). The barocycler was run at 35 °C, for 75 cycles with 60-sec pressure-cycle (50-sec high pressure, 10-sec ambient pressure, 25 kpsi). Subsequently, 4 μg trypsin was again added to each sample and digestion was repeated as mentioned above.

Further, to 110 μL of digested peptides sample, 10 μL of acetonitrile/water (1:1 v/v, containing 5% formic acid) was added to precipitate DOC. Samples were spun (10,000 rpm for 5 min at 10 °C) to remove the precipitate and 100 μL supernatant was collected. Finally, 25 μL of the

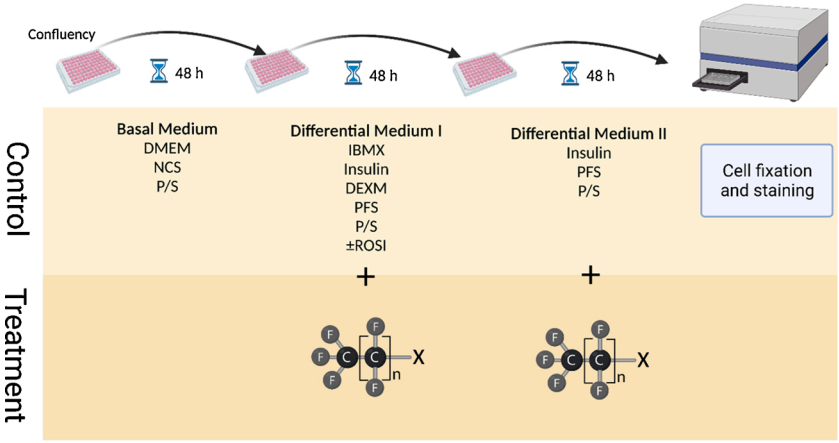

Fig. 1. Illustration of study design. Cells (5000/cm^2) were plated until they reach confluence. The cells first were cultured in Basal Medium I for two days and then they were differentiated for two days in differentiating medium I (DMI) and finally the differentiation was complete in differentiating medium II (DMII) for another two days. As it has been demonstrated, DMI included different concentration of IBMX, insulin, dexamethasone, PFS and antibiotics, while DMII only included insulin, PFS and antibiotics. Treatment with PFAS started at day two in DMI and continued for four days. Ten different PFAS with 3 different concentrations each was added along with three different concentrations of the differentiation cocktail in the presence or absence of rosiglitazone. Created with Biorender.com.

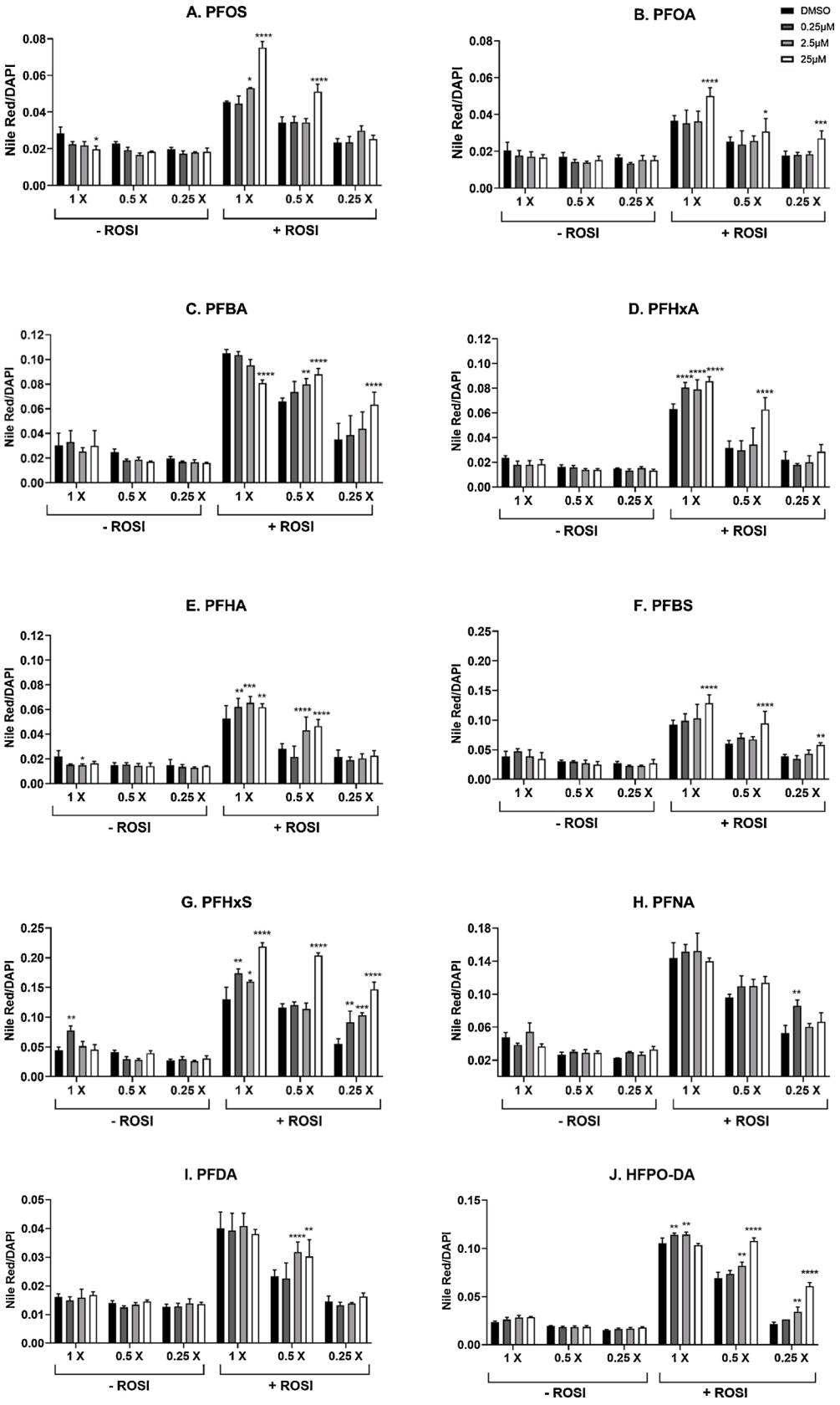

Fig. 2. Effect of PFAS on 3T3-L1 lipid content. Lipid content of cells exposed to 3 dilutions of the differentiating cocktail (1 X, 0.5 X, and 0.25 X) along with **A**) PFOS, **B**) PFOA, **C**) PFBA, **D**) PFHxA, **E**) PFHA, **F**) PFBS, **G**) PFHxS, **H**) PFNA, **I**) PFDA, and *J*) HFPO-DA at 0.25, 2.5, and 25 μM was determined using Nile Red staining. Nile-red florescent intensity was normalized to DAPI staining to account for difference in cell number. Calculations were performed using a one-way ANOVA followed by Fisher's LSD test to compare each PFAS treatment with its respective controls. All values are means ± SEM; n = 4. $p < 0.05$ *, $p < 0.01$ **, $p < 0.001$ ***, $p < 0.0001$ **** (For interpretation of the references to colour in this figure legend, the reader is referred to the web version of this article.).

digested peptide sample was injected on the analytical column and was analyzed using LC–MS/MS method described below.

2.5. Proteomics analysis

Data Indpendent Acquisition (DIA) or sequential window acquisition of all theoretical mass spectra (SWATH-MS) data acquisition methods were used as described previously with modifications (Jamwal et al., 2017). DIA was performed in positive ionization mode using a Duo-Spray™ ion source on a Sciex 5600 Triple TOF™ mass spectrometer (Sciex, Framingham, MA USA) equipped with an Acquity UPLC H Class system (Waters Corp., Milford, MA, USA). During the survey scan, all the ions between a mass range of *m/z* 300–1500 and exceeding 25 cps were used for MS/MS analysis. For product scan, data were acquired from 400−1100 *m/z* over 70 SWATH windows with a size of 10 Da each.

Chromatographic separation was achieved over 180 min gradient method at 100 µL/min on an Acquity UPLC Peptide BEH C18 (2.1 × 150 mm, 300 Å, 1.7 µm) preceded by an Acquity Van Guard pre-column (2.1 × 5 mm, 300 Å, 1.7 µm) (Waters Corp., Milford, MA, USA). Mobile phase A was water containing 0.1 % formic acid and mobile phase B was acetonitrile containing 0.1 % formic acid. Gradient conditions used were 98 % A from 0 to 5 min, 98 % to 70 % A from 5 to 155 min, 70 % to 50 % A from 155 to 160 min, 50 % to 5 % A from 160 to 170 min, 5 %–98 % A held from 170 to 175 min. The gradient was held at initial conditions from 175 min until the end of the run to equilibrate the column before the start of next run. The flow was diverted to waste for the first 8 min and last 20 min of the acquisition. Autosampler was maintained at 10 °C, and the column was kept at 50 °C. Trypsin-digested β-galactosidase peptides (Sciex, Framingham, MA USA) were injected to monitor TOF detector mass calibration.

2.6. Data processing

The raw data independent acquisition (DIA)-based proteomics was analyzed using Spectronaut (Ver. 13.10.191212.43655, Biognosys, Schlieren, Switzerland). The raw data first converted to HTRMS files using the Spectronaut Converter (Biognosys, Schlieren, Switzerland) and then direct data independent acquisition (DIA) was performed following generating spectral libraries by Pulsar and the murine FASTA file from UNIPROT. The default settings were used for the Spectronaut search. The output data from the Spectronaut was used to convert the raw intensity values to absolute protein level (pmol/mg protein) using the formula (Wisniewski and Rakus, 2014):

$$\text{Protein} = (\text{Total Intensity}/(\text{MW (g/mol)}*\text{Total Protein Intensity}))*10^9$$

Hierarchical clustering was performed using average Euclidean distance method (Perseus, Ver. 1.6.14.0) (Tyanova et al., 2016) and 3D Principal Component Analysis was created with the BioVinci software (BioTuring, San Diego, CA, USA) to depict the clusters of samples based on their similarity. The experiment of the cells treatment for the proteomics was performed in three sets (12 well plate, 5000 cell/cm^2) with different PFAS and vehicle as control. For comparisons between sample types, protein abundance was transformed to Log2 Fold Change (FC) where FC was determined as protein abundance with specific PFAS treatment/vehicle treatment. Subsequently, the filtering was done by applying statistical criteria of a 95 % up- or down-regulation likelihood (statistical *t*-test p-value < 0.05) and a fold-change threshold higher than 30 % (ratio of either <0.70 or >1.3) as significantly altered levels of expression which were selected for future pathway analysis and comparisons. The significant changes were investigated for major molecular and cellular functions with treatment of each PFAS using a core analysis on ingenuity pathway analysis software from Qiagen (Hilden, Germany) (Krämer et al., 2013).

2.7. Statistical analysis

Data were analyzed with one-way ANOVA followed by Fisher's LSD test using GraphPad Prism 9.1.2. All data are expressed as mean ± standard error of the mean (SEM). For LC–MS/MS SWATH data, t-tests were used to determine statistical differences. p-values less than 0.05 are reported as statistically significant. For all analyses, $p < 0.05$ *, $p < 0.01$ **, $p < 0.001$ ***, $p < 0.0001$ ****.

3. Results

3.1. PFAS induce 3T3-L1 cell differentiation to adipocytes

In general, treatment with the ten PFAS increased in Nile Red staining, with the presence of ROSI. With 1 X differentiating cocktail, PFOS increased lipid staining by 17 % and 66 % compared to control at 2.5 and 25 µM, respectively. When the dilution of the differentiating cocktail was decreased to 0.5 X, PFOS increased cellular lipid content by 49 % at a concentration of 25 µM (Fig. 2A). On the other hand, when the ROSI was not present, PFOS at 25 µM decreased the cellular lipid content by 30 % when the differentiating cocktail was not diluted 1 X. Moreover, in the presence of ROSI at the 1 X, 0.5 X, and 0.25 X dilutions, PFOA increased lipid content by 37 %, 22 % and 53 % compared to control at 25 µM, respectively (Fig. 2B).

Treatment with short chain carboxylic acids (PFBA, PFHxA, and PFHA) also produced an increase in lipid staining that was observed only in the presence of ROSI. PFBA increased lipid content by 21 % and 34 % with the concentrations of 2.5 and 25 µM, respectively at the 0.5 X dilution of the differentiating cocktail. At the 0.25X dilution, lipid content was also increased by 81 % at 25 µM (Fig. 2C). Treatment with PFHxA (Fig. 2D) with 1 X differentiating cocktail increased lipid content by 27 %, 25 %, and 35 % at concentrations of 0.25, 2.5 and 25 µM, respectively. When the differentiating cocktail was diluted to 0.5 X, PFHxA increased lipid content by 99 % at 25 µM. Treatment with PFHA (Fig. 2E) with 1X differentiating cocktail increased lipid content by 18 %, 24 % and 17 % at concentrations of 0.25, 2.5 and 25 µM, respectively. When the differentiating cocktail was lowered to the 0.5X dilution, PFHA increased lipid content by 52 % and 65 %, at 2.5 and 25 µM respectively. Overall, the short chain carboxylic acids (PFBA, PFHxA, and PFHA) increased lipid staining with the addition of ROSI to the media, the exception to this was when there was 1 X differentiating cocktail at the highest concentration of PFBA (25 µm), treatment with 25 µM of PFBA decrease lipid content by 23 %.

Short chain sulfonic acids (PFBS and PFHxS) also increased lipid staining in combination with ROSI addition to the media. At 25 µM of PFBS with ROSI, lipid content was increased in all the dilutions of differentiating cocktail (1 X, 0.5 X and 0.25 X), by 40 %, 58 % and 49 %, respectively (Fig. 2F). In Fig. 2G, PFHxS also increased lipid content. Without ROSI, the lipid content only increased in the presence of the undiluted differentiating cocktail (1 X) and the lowest concentration of PFHxS of 0.25 µM. With the addition of ROSI, PFHxS increased lipid content at all three concentrations (0.25, 2.5 and 25 µM), by 33 %, 22 %, and 68 % with undiluted differentiating cocktail (1 X), and by 66 %, 88 %, and 167 % with 0.25 X diluted differentiating cocktail, respectively. When the dilution of differentiating cocktail was 0.5 X, PFHxS significantly increased the lipid content only at a concentration of 25 µM.

Long chain carboxylic acid treatment (PFNA and PFDA) resulted in relatively less lipid accumulation overall compared to the PFAS tested at these concentrations. PFNA (0.25 µM) and ROSI increased lipid staining by 63 % with the 0.25 X dilution of the differentiating cocktail (Fig. 2H). PFDA only increased lipid content by 36 % and 29 % at concentrations of 2.5 and 25 µM, respectively in the presence of ROSI with a 0.5 X dilution of the differentiating cocktail (Fig. 2I).

As illustrated in Fig. 2J, HFPO-DA also increased the lipid content in the presence of ROSI. This increase was significant at 0.25 and 2.5 µM by 8 % and 8.5 % when the differentiating cocktail was undiluted (1 X).

Table 3
Summary of Lipid accumulation results at the selected treatment paradigm for proteomics.

PFAS	Change in lipid accumulation compared to untreated control	Fold-change
PFOS	↑	1.66
PFOA	↑	1.37
PFBA	↓	−1.30
PFHxA	↑	1.35
PFHA	↑	1.17
PFBS	↑	1.40
PFHxS	↑	1.68
PFNA	–	n/a
PFDA	–	n/a
HFPO-DA	–	n/a

Treatment paradigm for proteomics was selected 25 μM PFAS and differentiation cocktail dilution of 1 X with ROSI as 6 out of 10 had PFAS increased lipid content.

When the differentiating cocktail was diluted to 0.5 X, HFPO-DA increased lipid content by 18 % and 55 % at concentrations of 2.5 and 25 μM, respectively. When the differentiating cocktail was diluted to 0.25X, HFPO-DA increased lipid content by 61 % and 185 % at concentrations of 2.5 and 25 μM, respectively. Summary of lipid accumulation results at the selected treatment paradigm for proteomics has been summarized in Table 3.

3.2. Proteome analysis of adipocyte exposed to PFAS

After the treatment of cells with various PFAS for 96 h, the extraction of proteins and quantification was performed. Then, the proteins were enzymatically digested into peptides prior to MS analysis. In order to generate a comprehensive proteomic library, we used Spectronaut to process raw spectral counts. Then, the proteins with missing values were removed and the analysis was performed with the proteins left. With Spectronaut's internal normalization algorithm, we were able to identify 2405 proteins in PFBS, PFHxS, PFOS, PFOA, PFNA, PFDA and HFPO-DA run which became 2095 proteins after removing proteins with missing

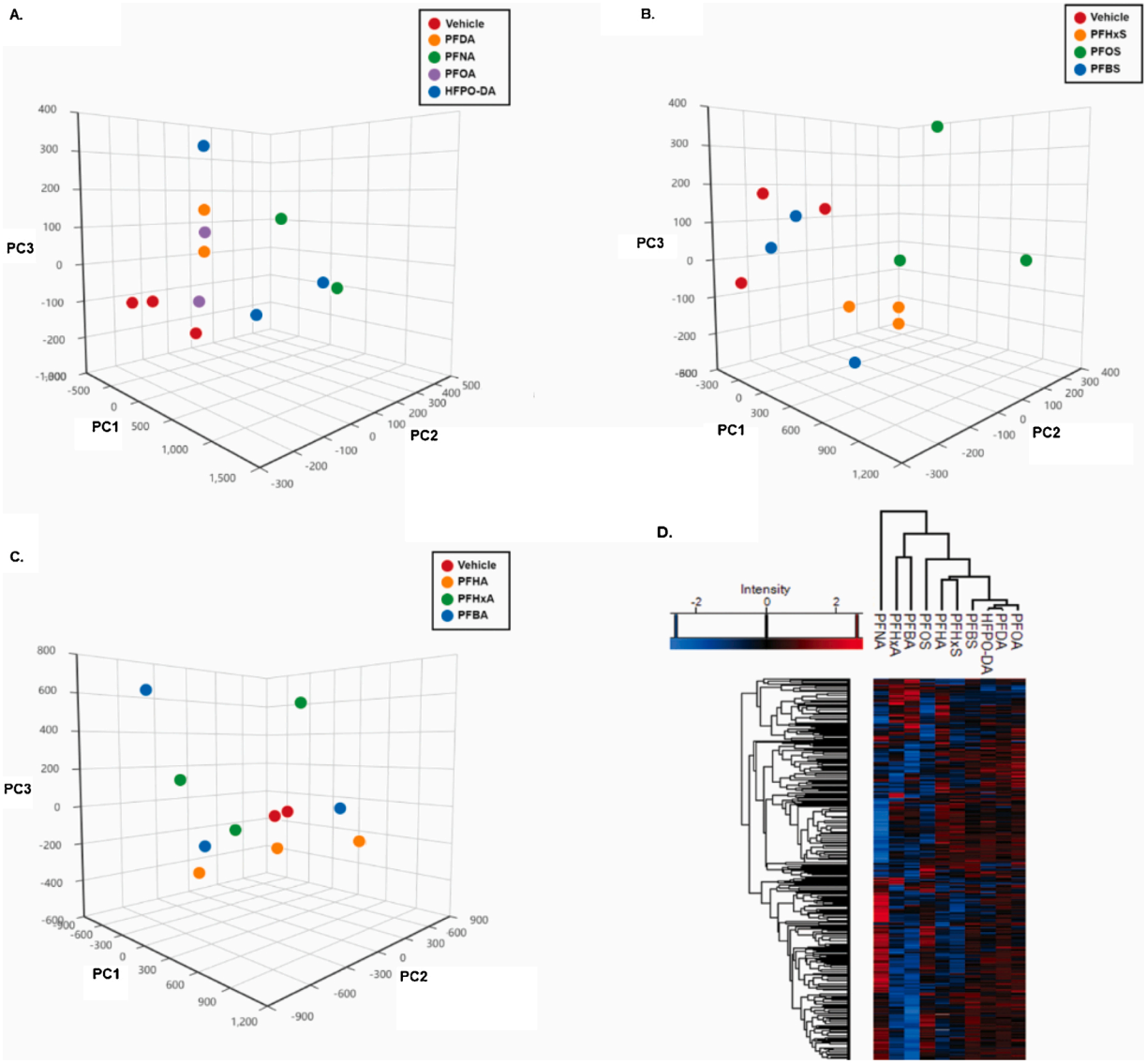

Fig. 3. PCA and hierarchical clustering of log 2-fold change in protein expression in response to ten different PFAS. The 3-dimensional image of PCA analysis of **A**) PFNA, PFDA, PFOA, HFPO-DA, **B**) PFHxS, PFOS, PFBS, and **C**) PFHA, PFHxA, and PFBA. The experiment was performed in three plates, with separate controls where n = 2 or 3. **D**) The column dendrogram associated with heatmap shows the hierarchical cluster of the treatment, where PFNA has the most unique protein expression profile compared to other PFAS.

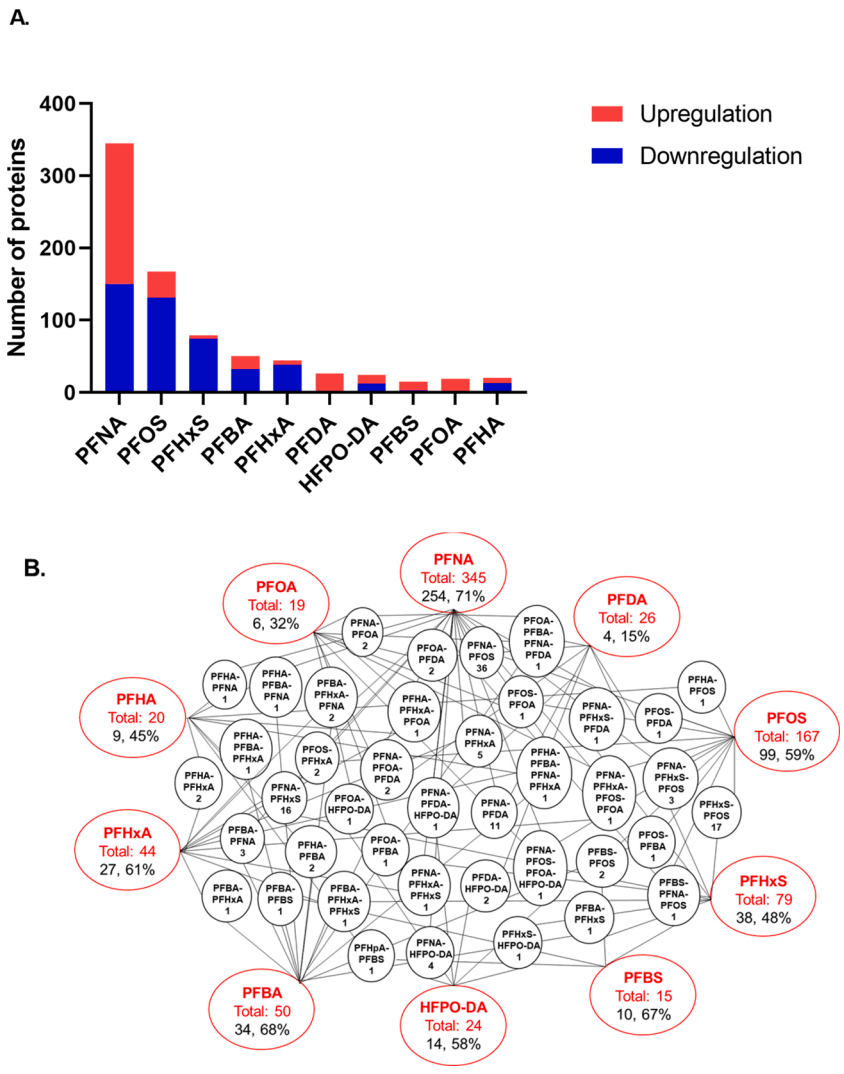

Fig. 4. Number of differentially expressed proteins in 3T3-L1 cells after treatment with different PFAS for four days during differentiation before proteomic analysis. A) The number of proteins upregulated or downregulated after treatment with each PFAS. B) The total number of unique and shared proteins that are up or downregulated for each PFAS treatment. For each of the PFAS, the total number of proteins with significantly altered level of expression has been determined in red. Also, the number of proteins which are unique and the percent of them as the result of the 3T3-L1 treatment with each PFAS has been shown with the red oval. Finally, the number of shared proteins significantly changed as a result of treatment with different PFAS has been shown in smaller central circles. As it can be seen, PFNA and PFOS have the highest number of differentially expressed. On the other hand, PFHA, PFDA and PFOA have the lowest number of differentially expressed proteins compared to other PFAS treatments (For interpretation of the references to colour in this figure legend, the reader is referred to the web version of this article.).

values. The number of proteins quantified with PFHA, PFBA and PFHxA run was 1277. As depicted in Fig. 3A–C, principal component analysis (PCA) of each group of samples treated with different PFAS showed specific clusters. In Fig. 3A, PFNA and PFDA show more clustering compared to other PFAS, and there is also a distinct cluster for PFOS as well in Fig. 3B. A heatmap of protein relative abundance (Fig. 3D) illustrates the clustering of the samples based on their expression profile. The results showed PFNA treatment had the most distinct expression profile from the treatment with other PFAS, followed by PFHxA, PFBA and PFOS. Filtering was performed by applying statistical criteria of a 95 % up- or down-regulation likelihood ($p < 0.05$ and a fold-change higher than 30 % (ratio of either <0.70 or >1.3) as significantly altered levels of expression. The number of proteins that have been either upregulated or downregulated has been summarized in the Fig. 4A, showing that PFNA is the PFAS that had most pronounced effect on the proteome of 3T3-L1 cells. PFNA had the largest number of upregulated proteins (195) and downregulated proteins (150). PFOS ranked second with upregulation of 36 proteins and downregulation of 131 proteins. After PFNA and PFOS, the PFAS that upregulated highest proteins were PFDA (24), PFBA (18), PFOA (17), PFBS (12), HFPO-DA (12), PFHA (7), PFHxA (6), and PFHxS (5) and the number of proteins downregulated with PFHxS, PFHxA, PFBA, PFHA, HFPO-DA, PFBS, PFOA and PFDA was 74, 38, 32, 13, 12, 3, 2 and 2 respectively. The number of either up- or downregulated proteins that are unique as a result of PFNA treatment was 71 % which was the largest. Following PFNA, PFBA had 68 % unique differentially expressed proteins. The percent of unique differentially expressed proteins for PFBS and PFHxA are 67 % and 61 %, respectively (Fig. 4B). The top three molecular and cellular functions resulted from the treatment of adipocytes with each PFAS was determined by analyzing significantly changed proteins with IPA. As seen in Table 4, the majority of cellular functions impacted are related to cell death, survival, and cellular organization. PFNA treatment impacted proteins involved in energy production and small molecule biochemistry. PFOS impacted proteins involved in nucleic acid metabolism, and PFDA and HFPO-DA impacted carbohydrate metabolism. Lipid metabolism cellular functions were affected only by treatment with PFOS, PFNA and PFBS. The markers involved in adipogenesis that have been significantly upregulated upon each PFAS exposure have been summarized in Table 5 and Fig. 5. It shows PFAS upregulated different markers during adipogenesis which caused increase in lipid content.

4. Discussion

In the current study, a 3T3-L1 cell line was used as a standard cell model to determine the potential toxicity of 10 common PFAS, including PFHA, PFBA, PFHxA, PFBS, PFHxS, PFOS, PFOA, PFNA, PFDA and HFPO-DA. Of the PFAS studied, PFDA, PFHxA, PFNA, PFOA, PFOS, PFHxS and HFPO-DA are among the PFAS detected in serum measurements of general U.S. population according to the Centers for Disease Control and Prevention (CDC) updates (CDC, 2021) The obesogen

Table 4
Top three molecular and cellular functions affected.

PFAS	Cellular function	p-value range
	Cell Death and Survival	7.08E-03 - 2.01E-06
PFOS	Lipid Metabolism	7.08E-03 - 3.45E-06
	Nucleic Acid Metabolism	7.08E-03 - 3.45E-06
	Cell-To-Cell Signaling and Interaction	4.77E-02 - 7.77E-04
PFOA	Cellular Assembly and Organization	3.88E-02 - 7.77E-04
	Cellular Maintenance	3.82E-02 - 7.77E-04
	Cell Cycle	5.00E-02 - 7.31E-04
PFBA	Cell Death and Survival	4.79E-02 - 7.31E-04
	Cell Morphology	1.09E-02 - 7.31E-04
	Cellular Assembly and Organization	4.91E-02 - 5.22E-04
PFHxA	Cellular Maintenance	4.91E-02 - 1.57E-03
	Cellular Movement	5.73E-03 - 1.57E-03
	Cell Morphology	1.71E-02 - 3.65E-04
PFHA	Cellular Compromise	1.16E-02 - 7.84E-04
	Cellular Maintenance	7.48E-04 - 7.48E-04
	Cell Cycle	1.93E-02 - 1.33E-04
PFBS	DNA Replication, Recombination, and Repair	1.93E-02 - 1.33E-04
	Lipid Metabolism	4.82E-02 - 4.16E-04
	Cellular Movement	2.84E-02 - 1.95E-06
PFHxS	Cellular Compromise	1.98E-02 - 3.26E-06
	Cell-To-Cell Signaling and Interaction	2.85E-02 - 1.08E-04
	Energy Production	2.90E-04 - 3.95E-14
PFNA	Lipid Metabolism	2.90E-04 - 3.95E-14
	Small Molecule Biochemistry	2.90E-04 - 3.95E-14
	Cellular Assembly and Organization	4.07E-02 - 6.62E-05
PFDA	DNA Replication, Recombination, and Repair	3.53E-02 - 6.62E-05
	Carbohydrate Metabolism	2.00E-02 - 1.44E-04
	Cellular Assembly and Organization	3.27E-02 - 4.71E-05
HFPO-DA	DNA Replication, Recombination, and Repair	3.00E-02 - 4.71E-05
	Carbohydrate Metabolism	3.42E-02 - 9.50E-04

Molecular and cellular functions resulted from the treatment of adipocytes with each PFAS was determined by analyzing significantly changed proteins with Ingenuity Pathway Analysis. Lipid metabolism pathway have been affected specifically by PFNA, PFOS and PFBS.

Table 5
List of regulatory factors associated with adipogenesis upregulated by PFAS.

Gene	PFAS	Adipogenesis effect	Reference
Ero1-Lα	PFHA and PFBA	Activation of PPARγ enhances Ero1-Lα expression and stimulates secretion of high molecular weight complexes of adiponectin in mature adipocytes	Qiang et al. (2007)
Nedd8	PFBA	Conjugates with PPARγ causing PPARγ stabilization	Park et al. (2016)
Mgst3	PFHxA	Adipocyte differentiation protein associated with acquisition of adipocyte phenotype	Jowsey et al. (2003)
Fitm2	PFHxS	Plays essential, physiological role in fat storage	Miranda et al. (2014)
Sod2	PFOS	Sod2 is correlated with diet induced obesity and insulin resistance	Han et al. (2016)
Bclaf1	PFOS	Interact with the leucine zipper region of C/EBPβ-Its direct role in adipocyte differentiation has not been investigated	Shao et al. (2016)
Dbi	PFOS	Indirect role in lipogenesis	Hansen et al. (1991)
Emd	PFOA	Decrease the stability of β-catenin and disruption of Wnt/β-catenin signaling pathway	Tilgner et al. (2009)
C3	PFNA	The product of complement C3, acylation stimulating protein (ASP), stimulates triacylglycerol synthesis in adipocytes	Scantlebury et al. (2001)
Sntb2	PFNA	Binds to utrophin and regulate lipid droplet size without affecting adipogenesis	Krautbauer et al. (2019)
Lgals1	PFNA	Interacts with PPARγ and increases its expression and transcriptional activation	Baek et al. (2021)

PPARγ, peroxisome proliferator-activated receptor gamma; Ero1-Lα, Ero-1 like protein alpha; Nedd8, neuronal precursor cell-expressed developmentally down-regulated protein 8 (NEDD8); Mgst3, microsomal glutathione S-transferase 3; Fitm2, fat storage inducing transmembrane protein 2; Sod2, Super oxide dismutase [Mn]; Bclaf1, Bcl-2 associated transcription factor 1; Dbi, Acyl-CoA-binding protein; Emd, emerin; C3, complement C3; Sntb2, beta-2-syntrophin; Lgals1, galectin-1.

hypothesis of PFAS is relatively new and unfortunately, robust *in vivo* methods to quantify the obesogenic effects of these compounds are currently lacking. The studies on adipogenic effects of PFAS have been mostly performed on *in vitro* systems and even those animal studies on the metabolic effects of these compounds are generally inconclusive (Heindel et al., 2015). PPARγ is highly expressed in adipocytes. Rosiglitazone is a well known agonist of PPARγ which significantly reduce the extent of plasma glucose by promoting adipogenesis leading to increased insulin sensitivity. Upon rosiglitazone binding, the PPARγ forms a heterodimer with the retinoid X receptor (RXR) which subsequently they bind to peroxisome proliferator response elements (PPRE) on several important target genes involved in carbohydrate and lipid metabolism which regulates adipocyte differentiation, glucose homeostatsis and lipid storage (Chiarelli and Di Marzio, 2008). Given the lack of comprehensive toxicological studies, in addition to long chain PFAS, short chain carboxylic acid and sulfonic acid PFAS along with HFPO-DA were characterized in this study for their potential of adipogenic differentiation. Three concentrations of a differentiating cocktail in the presence or absence of rosiglitazone, a PPARγ agonist were optimized to ensure lipid content changes induced by three different concentrations of PFAS would be detected. Moreover, given the wide range of PFAS concentrations detected in human population based on their occupational and geographical differences that play important role in the exposure, the PFAS adipogenesis potency with three different concentrations (0.25 μM to 25 μM) were evaluated (Olsen et al., 2007; Mamsen et al., 2019). Our findings suggest that in general the adipogenicity of PFAS could be highly complex. PPARγ is the most critical transcription factor and the master regulator of the differentiation of preadipocytes into adipocytes (Rosen et al., 1999). Treatment with PFAS during the differentiation stage in the medium free of rosiglitazone, didn't result in change in lipid content. The only PFAS that increased the adipogenesis significantly in the absence of rosiglitazone was PFHxS with the lowest concentration and highest concentration of differentiating cocktail. This trend in the absence of PPARγ agonist was expectable given the low concentration of PFAS that was considered in this study. Lipid accumulation and adipogenic differentiation has been promoted upon the exposure of very high concentrations of PFAS up to 100 μM (Qi et al., 2018) or 200 μM (Yamamoto et al., 2015). On the other hand, in the presence of rosiglitazone, as a general trend, increased lipid content is observed with increasing the concentration of PFAS from 0.25 to 25 μM. Given that none of the PFAS induced adipogenesis with no presence of ROSI, it can be concluded that the PFAS with the concentration range investigated in this study, have only the stimulating lipogenesis role of ROSI. For some PFAS that have been studied, it has been demonstrated that their agonistic activity on human PPARγ was significantly higher than that on mouse PPARγ. Takacs and Abbott found PFOA could activate human PPARγ but not the mouse PPARγ (Takacs and Abbott, 2007). Another trend observed was that in the presence of rosiglitazone, the lipid content was decreased with decreasing concentrations of differentiating agents. To the best of our knowledge, this is the most comprehensive study on the correlation between exposure and the adipogenicity potential of PFAS, which is especially important given their broad range of applications, high probability of getting exposed, and accumulative potential of the PFAS in human body. There are reports on adipogenesis and adipocyte differentiation of PFAS, but most studies are focused on PFOA and PFOS (Qi et al., 2018; Xu et al., 2016; Watkins et al., 2015; Yamamoto et al., 2015). PFBA, PFHxA, PFHA, PFNA, PFDA, PFBS, and PFHxS have also been found in human serum (Jakobsson et al., 2019), but there is little information in the literature regarding their adipogenic activity and potential to induce adipocyte

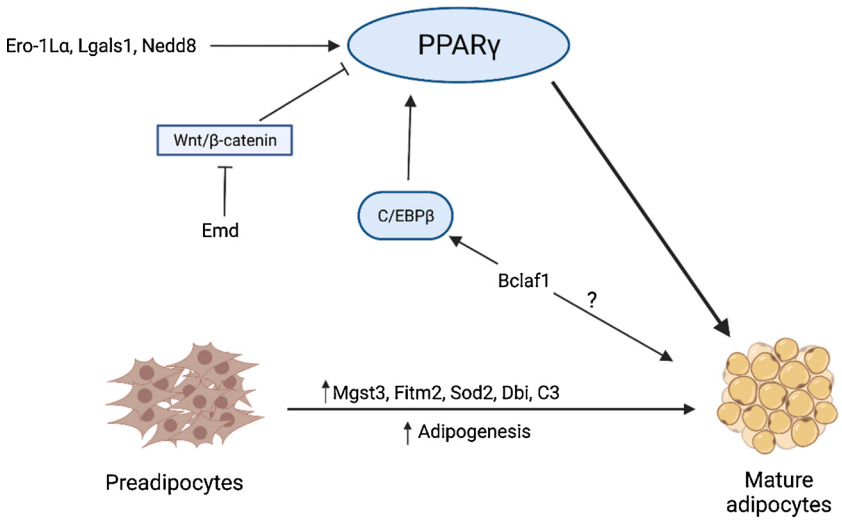

Fig. 5. Molecular regulation of peroxisome proliferator-activated receptor gamma (PPARγ). These signaling regulators have been significantly upregulated by treatment with different PFAS and detected by SWATH proteomics. They are directly or indirectly are involved in adipogenesis.

differentiation. It has been demonstrated that PFBS exposure also contributes to increased adipogenesis of 3T3-L1 adipocytes mostly during the early stage of adipogenesis, and that mitotic clonal expansion (MCE) was induced by PFBS treatment during this developmental interval. The suggested mechanism is that PFBS impacts adipogenesis, in part, *via* the upregulation of the MEK/ERK dependent pathway, which acts on MCE in the early stages of adipogenesis (Qi et al., 2018). Liu et al. studied the potential toxicity of four common short-chain PFAS, PFBS, PFHxS, PFBA and PFHxA, as replacements for PFOS and PFOA on human mesenchymal stem cells (hMSCs) demonstrated that although not as strongly as PFOS and PFOA, the four short-chain PFAS were capable of promoting hMSC adipogenic differentiation, resulting in more lipid accumulation (Liu et al., 2020). These studies show that short chain PFAS have the potential to induce adipogenesis in *in vitro* conditions. However, the data of adipogenesis resulted from the HFPO-DA should be interpreted cautiously because of its short half life in DMSO which degrades *via* decarboxylation to fluoroether E-1 (Beratore et al., 2020). In one study (Watkins et al., 2015), the authors evaluated the ability of PFAS to affect adipocyte differentiation and lipid accumulation; 3T3-L1 cells were treated with four perfluorinated compounds (PFOA, PFNA, PFHxS and PFOS), a PPARα agonist (WY-14,643), and a PPARγ agonist (rosiglitazone). The study demonstrated that treatment during the proliferation stage and subsequent differentiation stages in PPARγ rosiglitazone-free medium containing PFOA, PFNA, PFOS, and PFHxS caused an increase in cell number and lipid content although the pattern of effects on gene expression differed between the carboxylates (PFOA, PFNA) and the sulfonates (PFOS, PFHxS). This agrees with the present study, where different proteins involved in adipogenesis were upregulated compared to vehicle. The list of PFAS and the fold change of increasing lipid content that they have induced has been demonstrated in Table 3. With the differentiation cocktail of 1X and PFAS 25 μM, PFOS and PFHxS caused the highest level of increase in lipid content. Some proteins that are involved in adipogenesis which have been upregulated upon treatment with different PFAS have been summarized in Table 5 and Fig. 5. These are the proteins that directly or indirectly activate adipogenesis. For example, PFHA and PFBA both upregulated Ero1-Lα which is a target of PPARγ and stimulates secretion of adiponectin in mature adipocytes. In our study, PFNA treatment induced the highest modification in proteome expression compared to other PFAS. This result is in agreement with an *in vivo* study (Kudo et al., 2006) in mice, which concluded that the longer the carbon chain length becomes, the more potent were PFAS as inducers of hepatomegaly, peroxisomal β-oxidation and microsomal 1-acyl-GPC acyltransferase. The potency was in the order of PFNA > PFOA > PFHeA > PFHA. Despite much effort made in recent years to gain insight into the molecular regulation of adipogenesis, finding promising targets and identifying novel regulators of adipogenesis, including signaling pathways, remains elusive and crucial in the battle against obesity. A complex of hundreds of transcriptional factors which are involved in different signaling pathways play as either negative or positive modulators of adipose tissue development and adipogenesis (Guru et al., 2021). Determining the number of differentially expressed proteins specific for each PFAS showed PFNA caused 254 differentially expressed proteins, which was the highest number compared to the effect of all other PFAS. On the other hand, PFDA caused the differentially expression of 4 proteins specific to it. A study conducted on diabetic rats *in vivo* showed PFNA increased the activities of lipid synthesis, fatty acid synthase, glucose-6-phosphate dehydrogenase and decreased the activity of lipolytic enzyme, hepatic lipase, in the liver (Fang et al., 2015). The reason for observing different levels of adipogenesis and different effects on cellular metabolism upon exposure to different PFAS could be because of different affinities for the PPARγ and other transcriptions and signaling pathways involved in differentiation of fibroblasts to adipocytes. This is the first study that investigated the adipogenesis potency of different PFAS of various carbon chain length and functional group which can impact human health and environment. It showed the different potential of adipogenesis regarding these PFAS. However, this study provided only *in vitro* evidence for adipogenesis, but further *in vivo* and human studies are needed to confirm observations made herein. One limitation of *in vitro* study regarding PFAS is that FBS is available in media, and it is known that PFAS have a high affinity for albumin and this can affect the uptake and their intracellular availability during treatment (Bangma et al., 2020). Also, the study was limited by the proteome coverage and the analysis was based only on the proteins that were detected. Subcellular fractionation and protein enrichment techniques may be needed to allow better reproducibility and sensitivity.

5. Conclusion

In this study we evaluated 10 PFAS for the potential to induce murine 3T3-L1 fibroblast differentiation to adipocytes and induce lipid accumulation, as well as shift the cellular proteome. It is critical to understand the significance of PFAS on health and adipogenesis because of their vast spread in the environment, long half-life, and continued everyday usage. The results herein illustrate that PFNA caused the highest impact on the 3T3-L1 proteome profile and based on staining for

lipid droplets, short chain PFAS in specific concentrations along with differentiating agents show similar adipogenesis potential similar to PFOS and PFOA.

Declaration of Competing Interest

The authors declare that they have no known competing financial interests or personal relationships that could have appeared to influence the work reported in this paper.

Acknowledgements

This work was supported by National Institute of Health [grant number P42ES027706]. This material is based upon work conducted at a Rhode Island NSF EPSCoR research facility, Molecular Characterization Facility, supported in part by the National Science Foundation EPSCoR Cooperative Agreement # OIA-1655221, and at a Rhode Island Institutional Development Award (IDeA) Network of Biomedical Research Excellence from the National Institute of General Medical Sciences of the National Institutes of Health under grant number P20GM103430. The funders had no role in study design, data collection and analysis, decision to publish, or preparation of the manuscript.

The authors would like to thank URI LC-MS Proteomics Core for helping with DIA-SWATH study.

References

Ahmad, B., Serpell, C.J., Fong, I.L., Wong, E.H., 2020. Molecular mechanisms of adipogenesis: the anti-adipogenic role of AMP-activated protein kinase. Front. Mol. Biosci. 7, 76.

Antipatis, V.J., Gill, T.P., 2001. Obesity as a Global Problem. International Textbook of Obesity, pp. 3–22.

Baek, J.H., Kim, D.H., Lee, J., Kim, S.J., Chun, K.H., 2021. Galectin-1 accelerates high-fat diet-induced obesity by activation of peroxisome proliferator-activated receptor gamma (PPARγ) in mice. Cell Death Dis. 12, 66.

Baillie-Hamilton, P.F., 2002. Chemical toxins: a hypothesis to explain the global obesity epidemic. J. Altern. Complement. Med. 8, 185–192.

Bangma, J., Szilagyi, J., Blake, B.E., Plazas, C., Kepper, S., Fenton, S.E., Fry, R., 2020. An assessment of serum-dependent impacts on intracellular accumulation and genomic response of per- and polyfluoroalkyl substances (PFAS) in a placenta trophoblast model. Environ. Toxicol. 35, 1395–1405.

Beratore, H.K., Jackson, S.R., Strynar, M.J., McCord, J.P., 2020. Solvent suitability for HFPO-DA ("GenX"parent acid) in toxicological studies. Environ. Sci. Technol. Lett. 7, 477–481.

Blüher, M., 2019. Obesity global epidemiology and pathogenesis. Nat. Rev. Endocrinol. 15, 288–298.

US Centers for Disease Control and Prevention, 2021. National report on human exposure to environmental chemicals. https://www.CDC.gov.

Chawla, A., Schwarz, E.J., Dimaculangan, D.D., Lazar, M.A., 1994. Peroxisome proliferator-activated receptor (PPAR) gamma: adipose-predominant expression and induction early in adipocyte differentiation. Endocrinology 135, 798–800.

Chiarelli, F., Di Marzio, D., 2008. Peroxisome proliferator-activated receptor-gamma agonists and diabetes: current evidence and future perspectives. Vasc. Health Risk Manag. 4 (2), 297–304.

Christensen, K.Y., Raymond, M., Meiman, J., 2019. Perfluoroalkyl substances and metabolic syndrome. Int. J. Hyg. Environ. Health 222, 147–153.

Ciaraldi, T.P., Kong, A.P.S., Chu, N.V., Kim, D.D., Baxi, S., Loviscach, M., Plodkowski, R., Reitz, R., Caulfield, M., Mudaliar, S., Henry, R.R., 2002. Regulation of glucose transport and insulin signaling by troglitazone or metformin in adipose tissue of type 2 diabetic subjects. Diabetes 51, 30–36.

Conley, J.M., Lambright, C.S., Evans, N., McCord, J., Strynar, M.J., Hill, D., Medlock-Kakaley, E., Wilson, V.S., Earl Gray Jr., L., 2021. Hexafluoropropylene oxide-dimer acid (HFPO-DA or GenX) alters maternal and fetal glucose and lipid metabolism and produces neonatal mortality, low birthweight, and hepatomegaly in the Sprague-Dawley rat. Environ. Int. 146, 106204.

Danish Ministry of the Environment, 2015. Short-chain Polyfluoroalkyl Substances (PFAS). https://www2.mst.dk/Udgiv/publications/2015/05/978-87-93352-15-5.pdf.

Dassuncao, C., Pickard, H., Pfohl, M., Tokranov, A.K., Li, M., Mikkelsen, B., Slitt, A., Sunderland, E.M., 2019. Phospholipid levels predict the tissue distribution of poly- and perfluoroalkyl substances in a marine mammal. Environ. Sci. Technol. Lett. 6 (3), 9b00031.

Domingo, J.L., Nadal, M., 2019. Human exposure to per- and polyfluoroalkyl substances (PFAS) through drinking water: a review of the recent scientific literature. Environ. Res. 177, 108648.

Fang, X., Gao, G., Zhang, X., Wang, H., 2015. Perfluorononanoic acid disturbed the metabolism of lipid in the liver of streptozotocin-induced diabetic rats. Toxicol. Mech. Methods 25, 622–627.

Glüge, J., Scheringer, M., Cousins, I.T., DeWitt, J.C., Goldenman, G., Herzke, D., Lohmann, R., Ng, C.A., Trier, X., Wang, Z., 2020. An overview of the uses of per- and polyfluoroalkyl substances (PFAS). Environ. Sci. Process. Impacts 22 (12), 2345–2373.

Green, H., Kehinde, O., 1974. Sublines of mouse 3T3 cells that accumulate lipid. Cell 1, 113–116.

Guru, A., Issac, P.K., Velayutham, M., Saraswathi, N.T., Arshad, A., Arockiaraj, J., 2021. Molecular mechanism of down-regulating adipogenic transcription factors in 3T3-L1 adipocyte cells by bioactive anti-adipogenic compounds. Mol. Biol. Rep. 48, 743–761.

Han, Y.H., Buffolo, M., Pires, K.M., Pei, S., Scherer, P.E., Bou-dina, S., 2016. Adipocyte-specific deletion of manganese super-oxide dismutase protects from diet-induced obesity through increased mitochondrial uncoupling and biogenesis. Diabetes 65, 2639–2651.

Hansen, H.O., Andreasen, P.H., Mandrup, S., Kristiansen, K., Knudsen, J., 1991. Induction of acyl-CoA-binding protein and its mRNA in 3T3-L1 cells by insulin during preadipocyte-to-adipocyte differentiation. Biochem. J. 277, 341–344.

Heindel, J.J., Newbold, R., Schug, T.T., 2015. Endocrine disruptors and obesity. Nat. Rev. Endocrinol. 11, 653–661.

Itoh, T., Fairall, L., Amin, K., Inaba, Y., Szanto, A., Balint, B.L., Nagy, L., Yamamoto, K., Schwabe, J.W., 2008. Structural basis for the activation of PPAR gamma by oxidized fatty acids. Nat. Struct. Mol. Biol. 15, 924–931.

Jakobsson, K., Georgellis, K., Lilja, K., Norström, C., Nilsson, D., Pineda, C., Lind, H., 2019. Serum levels of a range of perfluorinated substances (PFAS) after drinking water exposure in three population living around military and civil airfields in Sweden. Environ. Epidemiol. 3, 179.

Jamwal, R., Barlock, B.J., Adusumalli, S., Ogasawara, K., Simons, B.L., Akhlaghi, F., 2017. Multiplex and label-free relative quantification approach for studying protein abundance of drug metabolizing enzymes in human liver microsomes using SWATH-MS. J. Proteome Res. 16 (11), 4134–4143.

Jowsey, I.R., Smith, S.A., Hayes, J.D., 2003. Expression of the murine glutathione S-transferasea3 (GSTA3) subunit is markedly induced during adipocyte differentiation: activation of the GSTA3 gene promoter by the pro-adipogenic eicosanoid 15-deoxy-12, 14-prostaglandin J2. Biochem. Biophys. Res. Commun. 312, 1226–1235.

Kotlarz, N., McCord, J., Collier, D., Lea, C.S., Strynar, M., Lindstrom, A.B., Wilkie, A.A., Islam, J.Y., Matney, K., Tarte, P., Polera, M.E., Burdette, K., DeWitt, J., May, K., Smart, R.C., Knappe, D.R.U., Hoppin, J.A., 2020. Measurement of novel, drinking water-associated PFAS in blood from adults and children in Wilmington, North Carolina. Environ. Health Perspect. 128, 077005.

Krämer, A., Green, J.J., Pollard, Tugendreich, S., 2013. Causal analysis approaches in ingenuity pathway analysis. Bioinformatics 30, 523–530.

Krautbauer, S., Neumeier, M., Haberl, E.M., Pohl, R., Feder, S., Eisinger, K., Rein-Fischboeck, L., Buechler, C., 2019. Theutrophin-beta 2 syntrophin complex regulates adipocyte lipid droplet size independent of adipogenesis. Mol. Cell. Biochem. 452, 29–39.

Kudo, N., Suzuki-Nakajima, E., Mitsumoto, A., Kawashima, Y., 2006. Responses of the liver to perfluorinated fatty acids with different carbon chain length in male and female mice: in relation to induction of hepatomegaly, peroxisomal b-oxidation and microsomal 1-acylglycerophosphocholine acyltransferase. Biol. Pharm. Bull. 29, 1952–1957.

Lau, C., Anitole, K., Hodes, C., Lai, D., Pfahles-Hutchens, A., Seed, J., 2007. Perfluoroalkyl acids: a review of monitoring and toxicological findings. Toxicol. Sci. 99, 366–394.

Liu, G., Dhana, K., Furtado, J.D., Rood, J., Zong, G., Liang, L., Qi, L., Bray, G.A., DeJonge, L., Coull, B., 2018. Perfluoroalkyl substances and changes in body weight and resting metabolic rate in response to weight-loss diets: a prospective study. PLoS Med. 15, e1002502.

Liu, S., Yang, R., Yin, N., Faiola, F., 2020. The short-chain perfluorinated compounds PFBS, PFHxS, PFBA, and PFHxA, disrupt human mesenchymal stem cell self-renewal and adipogenic differentiation. J. Environ. Sci. 88, 187–199.

Mamsen, L.S., Björvang, R.D., Mucs, D., Vinnars, M.T., Papadogiannakis, N., Lindh, C.H., Andersen, C.Y., Damdimopoulou, P., 2019. Concentrations of perfluoroalkyl substances (PFASs) in human embryonicand fetal organs from first, second, and third trimester pregnancies. Environ. Int. 124, 482–492.

Marques, E., Pfohl, M., Auclair, A., Jamwal, R., Barlock, B.J., Sammoura, F.M., Goedken, M., Akhlaghi, F., Slitt, A., 2020. Perfluorooctanesulfonic acid (PFOS) administration shifts the hepatic proteome and augments dietary outcomes related to hepatic steatosis in mice. Toxicol. Appl. Pharmacol. 408, 115250.

Miranda, D.A., Kim, J.H., Nguyen, L.N., Cheng, W., Tan, B.C., Goh, V.J., Tan, J.S.Y., Yaligar, J., Kn, B.P., Velan, S.S., Wang, H., Silver, D.L., 2014. Fat storage-inducing transmembrane protein 2 is required for normal fat storage in adipose tissue. J. Biol. Chem. 289, 9560–9572.

Olsen, G.W., Burris, J.M., Ehresman, D.J., Froehlich, J.W., Seacat, A.M., Butenhoff, J.L., Zobel, L.R., 2007. Half-life of serum elimination of perfluorooctanesulfonate, perfluorohexanesulfonate, and perfluorooctanoate in retired fluorochemical production workers. Environ. Health Perspect. 115, 1298–1305.

Olsen, G.W., Mair, D.C., Lange, C.C., Harrington, L.M., Church, T.R., Goldberg, C.L., Herron, R.M., Hanna, H., Nobiletti, J.B., Rios, J.A., Reagan, W.K., Ley, C.A., 2017. Per- and polyfluoroalkyl substances (PFAS) in American Red Cross adult blood donors, 2000–2015. Environ. Res. 157, 87–95.

Park, H.S., Ju, U.I., Park, J.W., Song, J.Y., Shin, D.H., Lee, K.H., Jeong, L.S., Yu, J., Lee, H.W., Cho, J.Y., Kim, S.Y., Kim, S.W., Kim, J.B., Park, K.S., Chun, Y.S., 2016. PPARγ neddylation essential for adipogenesis is a potential target for treating obesity. Cell Death Differ. 23, 1296–1311.

Qi, W.P., Clark, J.M., Timme-Laragy, A.R., Park, Y., 2018. Perfluorobutanesulfonic acid (PFBS) potentiates adipogenesis of 3T3-L1 adipocytes. Food Chem. Toxicol. 120, 340–345.
Qiang, L., Wang, H., Farmer, S.R., 2007. Adiponectin secretion is regulated by SIRT1 and the endoplasmic reticulum oxidoreductase Ero1-Lα. Mol.Cell. Biol. 27, 4698–4707.
Rangwala, S.M., Lazar, M.A., 2000. Transcriptional control of adipogenesis. Annu. Rev. Nutr. 20, 535–559.
Renner, R., 2001. Growing concern over perfluorinated chemicals. Environ. Sci. Technol. 35, 154A–160A.
Rosen, E.D., Sarraf, P., Troy, A.E., Bradwin, G., Moore, K., Milstone, D.S., Spiegelman, B. M., Mortensen, R.M., 1999. PPAR gamma is required for the differentiation of adipose tissue in vivo and in vitro. Mol. Cell 4, 611–617.
Scantlebury, T., Sniderman, A.D., Cianflone, K., 2001. Regulation by retinoic acid of acylation-stimulating protein and complement C3 in human adipocytes. Biochem. J. 356, 445–452.
Schulman, I.G., Shao, G., Heyman, R.A., 1998. Transactivation by retinoid X receptor peroxisome proliferator-activated receptor gamma (PPARgamma) heterodimers: intermolecular synergy requires only the PPARgamma hormone-dependent activation function. Mol. Cell. Biol. 18, 3483–3494.
Shao, A.W., Sun, H., Geng, Y., Peng, Q., Wang, P., Chen, J., Xiong, T., Cao, R., Tang, J., 2016. Bclaf1 is an important NF-kappaB signaling transducer and C/EBPbeta regulator in DNA damage-induced senescence. Cell Death Differ. 23, 865–875.
Takacs, M.L., Abbott, B.D., 2007. Activation of mouse and human peroxisome proliferator–activated receptors (α, β/δ, γ) by perfluorooctanoic acid and perfluorooctane sulfonate. Toxicol. Sci. 95 (1), 108–117.
Tilgner, K., Wojciechowicz, K., Jahoda, C., Hutchison, C., Mar-kiewicz, E., 2009. Dynamic complexes of A-type lamins and emerin influence adipogenic capacity of the cell via nucleocytoplasmic distribution of beta-catenin. J. Cell. Sci. 122, 401–413.
Tontonoz, P., Hu, E., Graves, R.A., Budavari, A.I., Spiegelman, B.M., 1994. mPPARγ2: tissue-specific regulator of an adipocyte enhancer. Genes Dev. 8, 1224–1234.
Tyanova, S., Temu, T., Sinitcyn, P., Carlson, A., Hein, M.Y., Geiger, T., Mann, M., Cox, J., 2016. The perseus computational platform for comprehensive analysis of proteomics data. Nat. Methods 13, 731–740.
U.S. Department of Health and Human Services, 2021. Public Health Service Agency for Toxic Substances and Disease Registry. www.atsdr.cdc.gov.
Watkins, A.M., Wood, C.R., Lin, M.T., Abbott, B.D., 2015. The eff ;ects of perfluorinated chemicals on adipocyte diff ;erentiation in vitro. Mol. Cell. Endocrinol. 400, 90–101.
Wisniewski, J.R., Rakus, D., 2014. Multi-enzyme digestion FASP and the 'Total Protein Approach'-based absolute quantification of the Escherichia coli proteome. J. Proteom. 109, 322–331.
Xu, J., Shimpi, P., Armstrong, L., Salter, D., Slitt, A.L., 2016. PFOS induces adipogenesis and glucose uptake in association with activationof Nrf2 signaling pathway. Toxicol. Appl. Pharmacol. 290, 21–30.
Yamamoto, J., Yamane, T., Oishi, Y., Kobayashi-Hattori, K., 2015. Perfluorooctanoic acid binds to peroxisome proliferator-activated receptor γ and promotes adipocyte differentiation in 3t3-l1 adipocytes. Biosci. Biotech. Biochem. 79, 636–639.
Yamashita, N., Kannan, K., Taniyasu, S., Horii, Y., Petrick, G., Gamo, T., 2005. A global survey of perfluorinated acids in oceans. Mar. Pollut. Bull. 51, 658–668.
Zhang, L., Ren, X.M., Wan, B., Guo, L.H., 2014. Structure-dependent binding and activation of perfluorinated compounds on human peroxisome proliferator-activated receptor γ. Toxicology 279, 275–283.